Preprints (www.preprints.org) | NOT PEER-REVIEWED | Posted: 22 December 2021 doi:10.20944/preprints202112.0359.v1

Article

Interfacial Stabilities, Electronic Properties and Interfacial Fracture Mechanism of 6H-SiC Reinforced Copper Matrix studied by the First Principles Method

Yao Shu [1,2,*], Shaowen Zhang [3,*],Yongnan Xiong [1,2], Xing Luo [1,2], Jiazhen He [1,2], Cuicui Yin [1,2], Xiaoyong Ding [4], Kaihong Zheng [1,2,*]

[1] Institute of New Materials, Guangdong Academy of Sciences, Guangzhou, 510651, Guangdong, China
[2] Guangdong Provincial Key Laboratory of Metal Toughening Technology and Application, Guangzhou, 510651, Guangdong, China
[3] School of Chemistry and Chemical Engineering, Key Laboratory of Cluster Science of Ministry of Education, Beijing Institute of Technology, South Zhongguancun Street #5, Haidian District, Beijing 100081, China
[4] School of Chemistry and Environmental Engineering, Sichuan University of Science and Engineering, Zigong 643000, Sichuan, China
* Correspondence: shuyao@gdinm.com (Y.S.); swzhang@bit.edu.cn (S.Z.); zhengkaihong@gdinm.com (K.Z.)

Abstract: The interfacial mechanics and electrical properties of the SiC reinforced copper matrix composites were studied via the first principles method. The work of adhesion (W_{ad}) and the interfacial energies were calculated to evaluate the stabilities of the SiC/Cu interfacial models. The carbon terminated (CT)-SiC/Cu interfaces were predicted more stable than those of the silicon terminated (ST)-SiC/Cu from the results of the W_{ad} and interfacial energies. The interfacial electron properties of SiC/Cu were studied via the charge density distribution, charge density difference, electron localized functions and partial density of the state. The covalent C-Cu bonds were formed based on the results of the electron properties, which further explained the fact that the interfaces of the CT-SiC/Cu are stable than those of the ST-SiC/Cu. The interfacial mechanics of the SiC/Cu were investigated via the interfacial fracture toughness and ultimate tensile stress, and the results indicate that both CT- and ST-SiC/Cu interfaces are hard to fracture. The ultimate tensile stress of the CT-SiC/Cu is nearly 23GPa, which is smaller than those of the ST-SiC/Cu of 25 GPa. The strains corresponding to their ultimate tensile stresses of the CT- and ST-SiC/Cu are about 0.28 and 0.26, respectively. The higher strains of CT-SiC/Cu indicate their stronger plastic properties on the interfaces of the composites.

Keywords: 6H-SiC; the first principles; copper matrix composites; electronic properties

1. Introduction

The copper metal composites have been extensively utilized in electronic technology [1], transportation [2]and aerospace fields [3]. Although the copper metal composites own high electrical conductivity, the weaker hardness and strength still limit their further applications. Therefore, copper alloy and copper matrix composites(CMCs) have been designed to improve their hardness and strength properties. However, as the reinforcement phase was introduced into the Cu matrix, the hardness and strength of the cooper materials are obviously enhanced [4,5]. Moreover, the reinforcements are the key factor of enhancing the mechanical properties for the CMCs without serious loss of the thermal and electrical properties of the matrix. Up to date, the reinforced phases including many types of ceramic materials, such as the carbide (TiC and WC) [6,7], the oxide (Al_2O_3, Y_2O_3) [8,9], and the ceramic (Ti_3AlC_2,AlN) [10,11] have already been employed to enhance the hardness and strength of the CMCs. Besides the ceramics discussed above, the iron [12] and its derivatives steel [13,14] were applied as the reinforcements for the copper matrix, which

© 2021 by the author(s). Distributed under a Creative Commons CC BY license.

Preprints (www.preprints.org) | NOT PEER-REVIEWED | Posted: 22 December 2021 doi:10.20944/preprints202112.0359.v1

not only for the high strength but also for the availability and low cost of the iron powder and iron based materials. Nevertheless, the carbon materials, such as diamond [15], graphite [16], carbon nanotubes (CNTs) [17] and graphene nano-sheets(GNSs) [18] have been developed as the reinforcements. Because the expensive price of CNTs, diamond and GNSs and the poor machinability of the diamond and the carbon materials, these carbon materials are still limited in the application as reinforcements.

Among these reinforcements, SiC is a potential and premium reinforcement for Cu matrix due to their special properties, which include the high hardness and high strength, excellent resistance during the processing of the oxidation and corrosion, low coefficient of thermal expansion and high heating transfer capabilities [19,20]. The SiC/Cu composites have aroused many scientists interested in its properties improving, which can be ascribe to their preeminent electrical [21], thermal conductivity [22], improved hardness [23], wear resistance [24], and frictional properties [25,26]. However, many experiments studied SiC/Cu composites adding different SiC content in copper. For example, Nalin Somani *et al.* found that the wear resistance capacity enhanced and the coefficient of friction reduced in SiC/Cu, which mainly due to the work of reinforcement SiC [27]. Rado, et al. found that Si atom diffuses into the matrix copper and a layer of carbon formed to stop the sufficient interfacial bonding [28]. According to Jarząbek *et al.* studies, SiC decomposed to Si and C in contact with copper during the sintering process [29]. Zhang L, *et al.* studied the SiC_P reinforced copper alloy composites, they found that $CuSi_5$, $CuSi_3$ and C were formed in the interfacial reactions and the products were confirmed by XRD tests [30]. Chen, G.Q *et al.* found that layered interfacial products were consisted by SiC particles, a Cu-Si layer, a polycrystalline C layer and Cu-Si matrix, but no $CuSi_3$ product was detected in these reacted regions [31]. Strojny-Nędza A, *et al.* studied the SiC/Cu composites by using the spark plasma sintering and Cu-SiC-Cu and systems were obtained, and they found that the copper reacts with the silicon carbide (6H-SiC type) during the processing of the annealing at a high temperature [32]. According to the discussions above, it can be found that the SiC/Cu interfacial investigation is very crucial to the properties of the SiC/Cu composites.

Besides the experiential investigation of the SiC/Cu composites, many theoretical studies were also performed on SiC/Cu composites by molecular dynamics. Zhou Yangguang *et al.* studied the mechanical behaviors of nanocrystalline SiC/Cu composites via the molecular dynamics (MD) simulations and they found that high strength and decent plasticity of metal matrix composites (MMC) could be obtained by adding the reinforcement which could be also working at the nanoscale [33]. Xiong et al. studied the defects generated by cooling of SiC/Cu composites by molecular dynamics, they found that cooling down from a higher temperature the magnitude of thermal residual stresses is higher, and more defects appear in the metal matrix [34]. Nevertheless, many works studied the interfaces and interfacial electronic properties via the first principles, such as TiC/Cu [35], TiB_2/Cu [36] and WC/Cu [37] copper matrix composites. The microelectronic properties of the interfacial atoms of the SiC/Cu have not been studied by the first principles method. The mechanism of the SiC reinforced Cu matrix at the micro level especially for electron properties are not clear.

Moreover, numbers of the hexagonal polytopes (4H and 6H-SiC) are utilized to be devices [38], due to their unique material properties such as high breakdown voltages, low leakage currents, large thermal conductivities and so on [39]. Nevertheless，the 6H-SiC with the anisotropy of the electron Hall mobility factor lager as 4.5 at the normal temperature [40]. Therefore, due to the high electron Hall mobility and premium properties of the 6H-SiC, we choose silicon carbide (6H-SiC) as our reinforcement for copper matrix composites.

In this theoretical studied, the interfacial properties such as interfacial interaction, stabilities of the heterogeneous interface of the SiC/Cu matrix composites had been studied via the first principles study. Moreover, according to the interfacial properties studies of the SiC/Cu, the work of adhesion, interfacial energies and ultimate tensile stress were

Preprints (www.preprints.org) | NOT PEER-REVIEWED | Posted: 22 December 2021 doi:10.20944/preprints202112.0359.v1

also studied to figure out the interactions between the SiC partical phase and copper matrix.

2. Computational Details

In order to construct the 6H-SiC/Cu heterogeneous interfacial models, (0001) and (111) crystal surfaces were utilized to build the SiC, Cu slab and SiC/Cu composites models, respectively. The convergence of the Cu and SiC slabs were tested for acquiring the suitable atomic layers to meet the interiors features of SiC and Cu bulks. Moreover, along the c axis direction for SiC and Cu surface slab a 15 Å vacuum layer were added to eliminate the interactions between the surface atoms. In addition, for the sake of considering all possibilities of the SiC/Cu interfaces, the different stacking ways of Cu, the interior structures of SiC and different atomic terminations (carbon terminated (CT) and silicon terminated (ST)) at the surfaces needing to be involved. Therefore, there are totally 18 types of SiC/Cu models displayed in **Fig. 1**. The stacking ways of the Cu atoms in Cu slabs along with the SiC surface, i.e., "HCP", "MT" and "OT" stacking ways were involved, in which "HCP" stacking way means: the interfacial Cu atoms placed on-top the first layer of SiC atoms; "MT" stacking way means: the interfacial Cu atoms which are reside atop of the connection midpoint of the first layer SiC atoms; "OT" stacking way means: the interfacial Cu atoms which are reside atop the second layer SiC atoms. Moreover, owing to the interior structure of the SiC, there are three different structurers connected with the interfacial Cu slab atoms, *viz.* "(a)" "(b)" and "(c)". The "(a)" of the 6H-SiC refers to the interfacial atoms C or Si (terminated) reside atop the midpoint of the atomic connection of the first layer of Cu atoms,

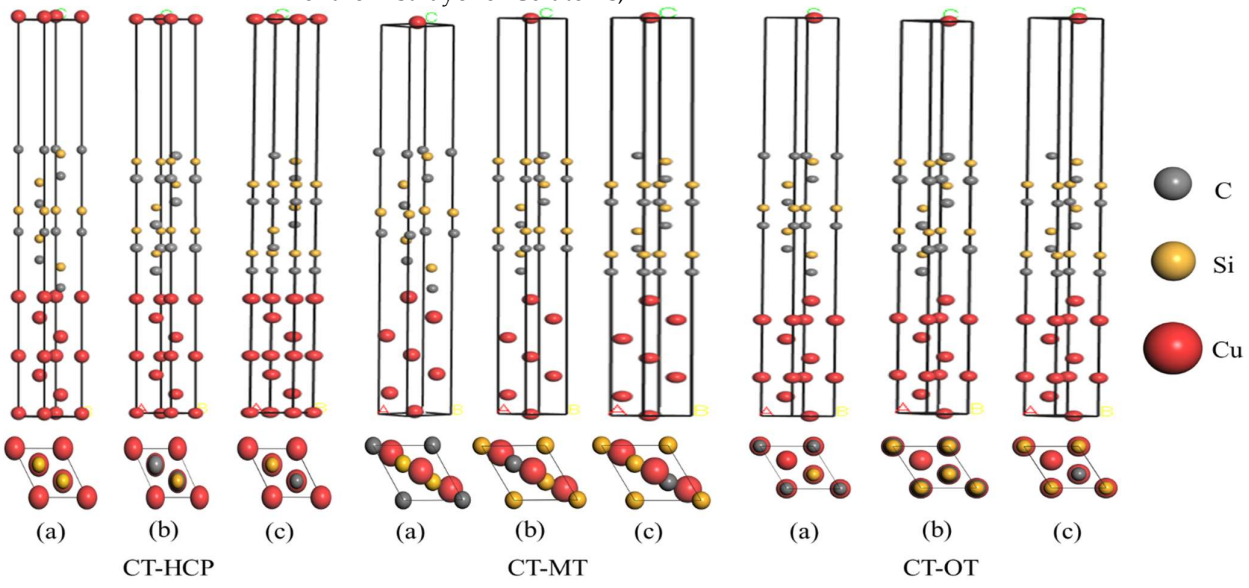

(a)

Preprints (www.preprints.org) | NOT PEER-REVIEWED | Posted: 22 December 2021 doi:10.20944/preprints202112.0359.v1

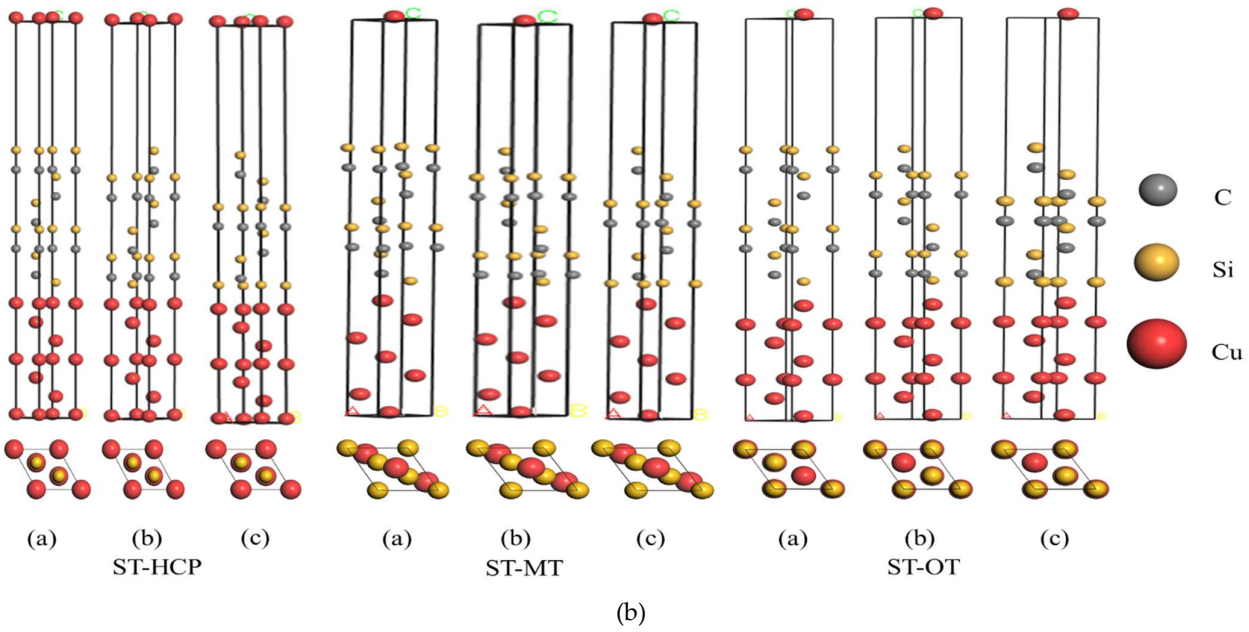

Figure 1. 6H-SiC Reinforced Copper Matrix Composites Models: (a) Carbon terminated (CT)-6H-SiC(0001)/Cu(111) interfacial models, (b) Silicon terminated (ST)-6H-SiC(0001)/Cu(111) interfacial models. Above graphs are side view of the 6H-SiC(0001)/Cu(111), under the side view graphs is the top view of the 6H-SiC(0001)/Cu(111).

"(b)" is invers of the structure "(a)", and "(c)" means that the interfacial C or Si atoms are connected on-top of the first layer Cu atoms. In general, three different Cu stacking sequences (HCP, OT and MT), three combined ways of SiC ((a), (b) and (c)) and two terminated Si and C atoms of the SiC slab at the surfaces were taken into account.

All calculations were based on the periodic boundary conditions and plane wave basis set and which carried out by the Cambridge Serial Total Energy Package Code (CASTEP) [41,42]. The Perdew-Burker-Enzerhof (PBE) functional generalized gradient approximation (GGA) [43] were performed to manage the exchange-correlation interactions. Moreover, the Monkhorst-Pack k-point grid [44] 11×11×1 was sampled with the Brillouin zone for the SiC/Cu, Cu and SiC slab, respectively. The Broyden-Fletcher-Goldfarb-Shanno (BFGS) [45] algorithm was applied to relax the atomic structures to reach the ground state. The 500 eV was chosen as the expansion in reciprocal space for cut-off energy of the plane wave. Nevertheless, the total energy tolerance, maximum force tolerance and maximal displacement such calculating convergent parameters were performed by 1.0×10^{-5} eV/atom, 0.03 eV/Å and 1.0×10^{-5} Å, respectively. The valence electrons of $3s^2 3p^2$, $2s^2 2p^2$ and $3s^2 3p^6 3d^2 4s^2$ were considered for the Si, C and Cu atom pseudopotentials. In addition, for all 6H-SiC/Cu interfacial models, 18 atoms were included during the whole processing of calculations.

3. Results and Discussion

3.1. Bulk properties

The fcc-Cu and 6H-SiC cells were optimized via GGA-PBE method [43] to evaluate the proper parameters, our calculated and the reported cell parameters listed in **Table 1**. The 6H-SiC belongs to the $P6_{3mc}$ space group and its cell parameters are $a = b = 3.095$ Å, c=15.185 Å, $\alpha = \beta = 90°$, $\gamma = 120°$, respectively. After optimization of the 6H-SiC cell, our calculated 6H-SiC cell parameters are $a = b = 3.085$ Å, $c = 15.123$ Å, $\alpha = \beta = 90°$, $\gamma = 120°$, closed to the reported values in **Table 1**.

Table 1. The simulative and experimental cell parameters of the 6H-SiC and Cu bulks.

Bulks	Method	*a* (Å)	*c* (Å)	V_o

Preprints (www.preprints.org) | NOT PEER-REVIEWED | Posted: 22 December 2021 doi:10.20944/preprints202112.0359.v1

6H-SiC	GGA[this work]	3.085	15.123	143.93
	GGA [47]	3.078	15.114	143.19
	GGA [48]	3.079	15.110	143.25
	GGA [49]	3.081	15.117	143.50
	GGA [50]	3.09	15.17	144.85
	Exp. [51]	3.08	15.08	143.05
Cu	GGA[this work]	3.628	3.628	47.77
	GGA [35]	3.627	3.627	47.71
	GGA [52]	3.636	3.636	48.07
	GGA [53]	3.631	3.631	47.87
	Exp. [54]	3.615	3.615	47.24

3.2. The Convergent tests of the 6H-SiC (0001) and Cu (111) slab.

The layer thickness was initially determined by testing the change of the layer distances, until the optimization of SiC (0001) and Cu (111) slab reached the convergence at the proper atomic layers. On the one hand, the results of the calculation might be inaccurate if atomic layers were too less. On the other hand, much time and resources would be spent if atomic layers were too large. Therefore, in order to acquire the approximate properties of the bulk for slab interior, the proper atomic layers of the slabs need to be pretested initially. The Δ_{ij} is applied to determine the layer thickness of the slab and which can be defined in **Eq. (1)**. In **Eq. (1)**, where d_{ij} refers to the spacing between the neighboring *i* and *j* layers of the crystal before the relaxation, d'_{ij} is the spacing between the neighboring *i* and *j* layers after relaxation. The calculated convergent results are listed in **Table 2**, in which the CT and the ST of the 6H-SiC slabs achieved the convergence with the tiny Δ_{ij} values respecting to above 11 (for CT Δ_{34} is -0.97% , for ST Δ_{34} is -0.18%) SiC and 7(Δ_{23} is 0.72%) Cu layer thickness.

In specific, the calculated Δ_{ij} values for all ST-6H-SiC layer thickness (most Δ_{ij} are lower than absolute value |0.5%|) are much lower than those of the CT-6H-SiC layer thickness, which show that the former are more inclined to be convergent than those of the latter. In addition, it can

Table 2. 6H-SiC (0001) and Cu (111) surface relaxations as a function of termination and slab thickness.

Surfaces	Interlayer	Slab thickness, Δ_{ij} (%)					
		n 3	5	7	9	11	13
ST-6H-SiC(0001)	Δ12	-1.13	-0.08	-0.21	-0.16	-0.21	-0.22
	Δ23		1.34	0.09	0.03	-0.10	-0.16
	Δ34			-0.19	-0.19	-0.18	-0.30
	Δ45				0.08	-0.18	-0.35
	Δ56					-0.32	-0.42
	Δ67						-0.49
CT-6H-SiC(0001)	Δ12	-11.0	-3.69	-5.83	-6.47	-6.55	-6.51
	Δ23		5.07	2.33	2.28	2.57	2.20
	Δ34			-1.10	-1.56	-0.97	-1.49
	Δ45				-0.37	-0.37	-0.24
	Δ56					-0.09	-0.55
	Δ67						-0.18
Cu(111)	Δ12	1.32	0.33	0.59	0.92	0.07	-0.13
	Δ23	-	0.68	0.72	1.04	1.01	0.85
	Δ34	-		0.89	1.32	0.53	1.05

Preprints (www.preprints.org) | NOT PEER-REVIEWED | Posted: 22 December 2021 doi:10.20944/preprints202112.0359.v1

	Δ45	-	1.08	0.72	0.88
	Δ56	-		0.74	0.79
	Δ67				0.75

$$\Delta_{ij} = \frac{d'_{ij} - d_{ij}}{d_{ij}} \times 100\% \quad (1)$$

be found that after 11 atomic layers of ST-6H-SiC layer slab, the Δ_{ij} values are gradually reduced and their properties of the interior layers are more tended to reach those of the bulk materials. Nevertheless, when layer thickness of CT-6H-SiC above 9 (for 9 layer thickness their Δ_{23} and Δ_{34} are respective as 2.28% and -1.56%), their interior slab properties are more inclined to be the properties of the 6H-SiC bulk, for the subtle difference of the Δ_{ij} values. The similar situations happen to Cu(111) slab when the layer thickness are above than 7. Therefore, 11 and 7 atomic layer thickness of SiC and Cu were chosen to construct the SiC/Cu interfacial models.

3.3. Interfacial and surface energy

3.3.1. The 6H-SiC (0001) surface energy

Owing to the hard directive detection of the 6H-SiC/Cu interfacial structure of the experiments, the simulative calculation is a useful method to analyze the interfacial structures details of the composites. The Si and C chemical potentials need to be considered when the 6H-SiC (0001) slab surface energies studied, because the polarization of SiC surfaces slab caused by these two types atoms. As a result, 6H-SiC (0001) surface plane can be divided into two components *viz.*, ST and CT-surface. The surface energy (γ_s) can be defined in subsequent equation:

$$\gamma_s = (E_{slab} - N_{Si}\mu_{Si}^{slab} - N_C\mu_C^{slab} + PV - TS)/2A \quad (2)$$

where E_{slab} refers to the total energy of the relaxed surface structure, μ_{Si}^{slab} and μ_B^{slab} represent the chemical potential of Si and C atoms, N_{Si} and N_C are the number of the Si and C atoms in corresponding slab, and A is the surface area of the interfacial model. Moreover, the pattern *PV* and *TS* can be neglect at the specific pressure and 0 K. When 6H-SiC bulk and SiC (0001) slabs were fully relaxed, they both reached the equilibrium state. In **Eq. (3),** and **Eq. (4)**, where ΔH_{SiC} stands for the heat formation of the bulk SiC, μ_{SiC}^{bulk}, μ_{SiC}^{slab}, μ_{Si}^{bulk} and μ_C^{bulk} refer to the chemical potential of the 6H-SiC bulk, SiC (0001) slab, Si bulk and C bulk, respectively. However, the ΔH_{SiC} obtained in this study is -0.325 eV/until per cell. **Eq. (5)** is acquired by substituting **Eq. (3)** and **Eq. (4)** into **Eq. (2)**.

$$\mu_{SiC}^{slab} = \mu_{Si}^{slab} + 2\mu_C^{slab} \quad (3)$$

$$\mu_{SiC}^{bulk} = \mu_{Ti}^{bulk} + \mu_C^{bulk} + \Delta H_{SiC} \quad (4)$$

$$\gamma_s = [E_{slab} - N_C\mu_{SiC}^{bulk} + (N_C - N_{Si})\mu_{Si}^{buk}]/2A \quad (5)$$

Because the chemical potential of each element in the bulk is lower than that in the slab, the difference of the chemical potential for each element ($\Delta\mu$) can be expressed via the following inequalities:

Preprints (www.preprints.org) | NOT PEER-REVIEWED | Posted: 22 December 2021 doi:10.20944/preprints202112.0359.v1

$$\Delta\mu_{Si} = \mu_{Si}^{slab} - \mu_{Si}^{bulk} \leq 0 \quad (7)$$

$$\Delta\mu_{C} = \mu_{C}^{slab} - \mu_{C}^{bulk} \leq 0 \quad (8)$$

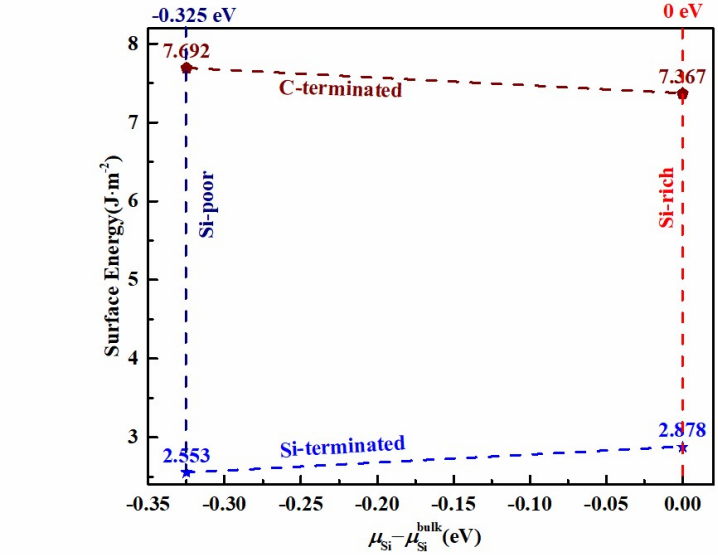

Figure 2. Surface energy of 6H-SiC(0001) respect to Si chemical potential change.

$$\Delta H_{SiC} \leq \mu_{Ti}^{slab} - \mu_{Ti}^{bulk} \leq 0 \quad (9)$$

The ST and CT-6H-SiC(0001) surface energies were calculated over the entire range of Si chemical potentials. Compared with the previous studies, our calculated 6H-SiC(0001) surface energies are respective as 2.553-2.878 J·m^{-2} (ST) and 7.367-7.692 J·m^{-2} (CT), which are a bit lower than the reported values 3.22 J·m^{-2} (ST) and 7.82 J·m^{-2} (CT)[31]. In addition, the reported 4H-SiC(0001) surface values are 2.899-3.535 J·m^{-2} for Si-terminated and 7.783-8.426 J·m^{-2} [55] for C-terminated. (other reported results are (2.86-3.52 for Si-terminated and 7.92-8.59 for C-terminated)) [56] which are very close to our calculated results.

3.3.2. The surface energy of the Cu (111)

The surface energy of Cu (111) have been studied in many previous work, and their values are displayed in **Table 3**. Comparing with these surface energies, the Cu (111) surface energy is 1.39 J·m^{-2} calculated in this work, which closing to the reported values 1.32 J·m^{-2} [29],1.36 J·m^{-2} [30]and 1.40 J·m^{-2} [57], but higher than study results over the two decades (1.2 J·m^{-2} and 2.07 J·m^{-2}) [58,29].

Table 3. The calculated surface energy of the Cu (111).

Entry	Surface energy (J·m^{-2})					
Cu (111)	1.39$^{\text{this work}}$	1.32 [35]	1.36 [36]	1.2 [58]	1.40 [57]	2.07 [59](unrelaxed)

3.3.3. Work of adhesion (W_{ad}) and interfacial distance

The work of adhesion (W_{ad}) is utilized to evaluate the stabilities of the heterogeneous interfaces, which can be expressed as the work of separation when heterogeneous

Preprints (www.preprints.org) | NOT PEER-REVIEWED | Posted: 22 December 2021 doi:10.20944/preprints202112.0359.v1

interfaces divided into the two free independent parts. Therefore, the W_{ad} can be defined in the subsequent equation:

$$W_{ad} = -(E^{total}_{SiC/Cu} - E^{slab}_{SiC} - E^{slab}_{Cu}) / A = (E^{slab}_{SiC} + E^{slab}_{Cu} - E^{total}_{Si/Cu}) / A \quad (10)$$

In **Eq. 10**, where $E^{total}_{Si/Cu}$, E^{slab}_{SiC} and E^{slab}_{Cu} represent the total energy of the SiC(0001)/Cu(111) composites, the total energy of the relaxed individual separated SiC (0001) and Cu (111) slabs in identical supercells, respectively. The A represent to the area of the interfacial surface of the SiC(0001)/Cu(111) composites.

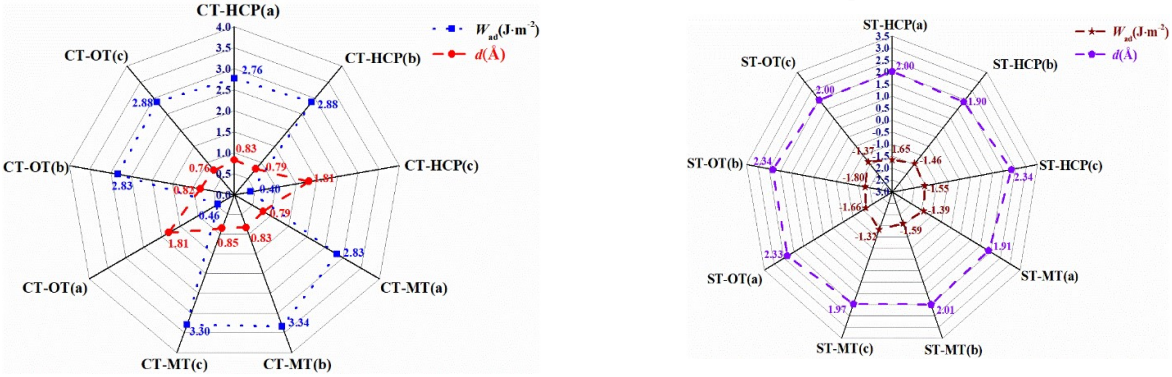

(a) (b)

Figure 3. Interfacial distance and work of adhesions for 6H-SiC(0001)/Cu(111): **(a)** CT-6H-SiC(0001)/Cu(111) interfaces **(b)** ST-6H-SiC(0001)/Cu(111) interfaces.

In **Fig. 3 (a),** all W_{ad} values are positive and which are various from 0.4 J·m^{-2} to 3.34 J·m^{-2}. Among the CT-6H-SiC(0001)/Cu(111) interfacial models, CT-MT(b) (3.34 J·m^{-2}) and CT-HCP(c) (0.40 J·m^{-2}) have the largest and the smallest W_{ad}, while for other interfacial models, the W_{ad} values are between these two extremes. The opposite situation happened to ST-6H-SiC(0001)/Cu(111) interfaces. In **Fig. 3 (b),** W_{ad} of the ST-6H-SiC(0001)/Cu(111) interfaces are all negative and which different from -1.80 J·m^{-2} to -1.32 J·m^{-2}. The stabilities of the CT-6H-SiC(0001)/Cu(111) interfaces are stronger than those of the ST-6H-SiC(0001)/Cu(111), due to the strong interactions of the CT-6H-SiC(0001)/Cu(111) (W_{ad} are positive) and the weak interactions of the ST-6H-SiC(0001)/Cu(111) (W_{ad} are negative).

In addition, interfacial distances of CT-6H-SiC(0001)/Cu(111) are larger than those of the ST-6H-SiC(0001)/Cu(111) in **Fig. 3 (a) (b)**, and the average distance of the former is only 0.85 Å contrasting to the large average distance 2.0 Å of the latter. In specific, the most unstable interface CT-HCP(c) (0.4 J·m^{-2}) own the largest interfacial distance 1.81 Å, and similar ST-OT(b) has the largest interfacial distance (2.34 Å) corresponding to its lowest W_{ad} value (-1.81 J·m^{-2}).

3.3.4. 6H-SiC(0001)/Cu(111) interfacial energies

The stabilities of the heterogeneous interfaces can be evaluated via the interfacial energy. However, the assessment format of the interfacial energy is different with the work of adhesion, namely, the larger of the interfacial energies, the weaker of the interface stabilities. The interfacial energy can be defined in the following equation for the 6H-Si(0001)/Cu(111) composite models:

$$\gamma_{int} = \gamma_{Cu(111)} + \gamma_{SiC(0001)} - W_{ad} \quad (11)$$

In **Eq. (11)**, where γ_{int}, $\gamma_{Cu(111)}$, $\gamma_{SiC(0001)}$ and W_{ad} are represent the interfacial energy of the 6H-SiC(0001)/Cu(111), surface energy of the Cu(111), surface energy of the 6H-SiC(0001) and work of adhesion of the 6H-SiC(0001)/Cu(111), respectively.

Preprints (www.preprints.org) | NOT PEER-REVIEWED | Posted: 22 December 2021 doi:10.20944/preprints202112.0359.v1

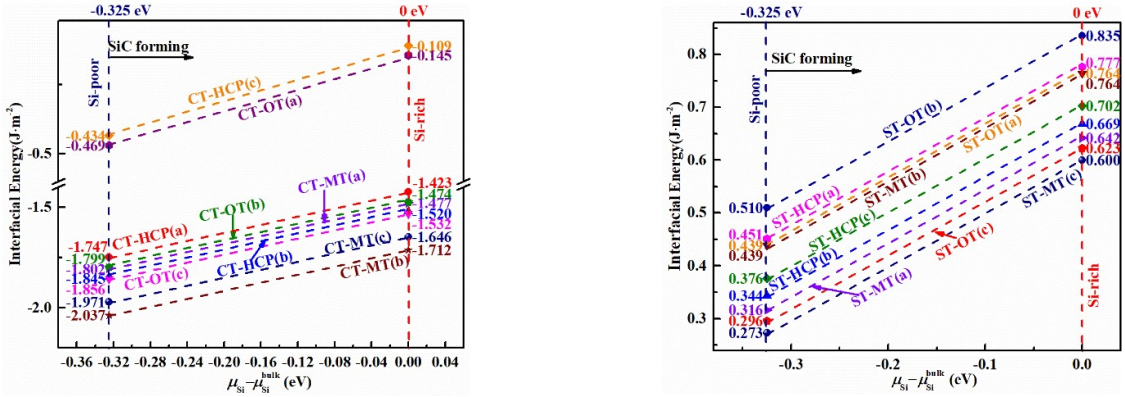

Figure 4. The interfacial energy of the 6H-SiC/Cu composite models: (a) CT-6H-SiC(0001)/Cu(111) interfacial energies (b) ST-6H-SiC(0001)/Cu(111) interfacial energy.

According to **Fig. 4 (a)**, all CT-6H-SiC(0001)/Cu(111) interfacial energies are negative contrasting with the positive interfacial energies of the ST-6H-SiC(0001)/Cu(111) , which further ensure that the CT-6H-SiC(0001)/Cu(111) interfaces are more stable than those of the ST-6H-SiC(0001)/Cu(111) interfaces. Specifically, the CT-MT(b) has the lowest interfacial energy (-1.712 J·m^{-2}~ -2.037 J·m^{-2}) and the highest W_{ad} (3.34 J·m^{-2}), performing the most stable interface among all CT-6H-SiC(0001)/Cu(111) interfacial models. In the same way, the largest interfacial energy (0.510~0.835 J·m^{-2}) and lowest W_{ad} values (-1.81 J·m^{-2}) of the ST-OT(b) own the weakest stable interface among the ST-6H-SiC(0001)/Cu(111) interfacial models. In general, the sequence of the 6H-SiC(0001)/Cu(111) interfacial energies from the large to the small corresponding to the sequence of the W_{ad} from the small to the large, which verified that the results obtained via these two methods are consistent well.

4. Interfacial atom electronic properties of the 6H-SiC(0001)/Cu(111) composites.

The electronic properties of the 6H-SiC(0001)/Cu(111) interfacial atoms have been analyzed via the charge density distribution, the charge density difference and the electron localized function methods. Based on these methods, the charge density distribution is in consideration of the total electrons state of each atom, the charge density difference is in view of the charge communications between the two neighborhood atoms and the electron localized function is taken account of the atom bonding state. Furthermore, the partial density of state (PDOS) of the 6H-SiC(0001)/Cu(111) interfacial atoms are analyzed by their atomic orbital electrons densities. Among all 6H-SiC(0001)/Cu(111) interfacial models, six of them (CT-HCP(a),CT-MT(a),CT-OT(a),ST-HCP(a),ST-MT(a) and ST-OT(a)) were discussed , and other calculated models could been seen in **Fig. SI(1)** to **Fig. SI(6),** respectively.

4.1. The charge density distributions of the 6H-SiC(0001)/Cu(111) interfacial atoms.

As shown in **Fig. 5 (a), (b), (c)**, abundant charges assembled between the interfacial C and Cu atoms, which indicate that the strong interactions happened on these interfaces. However, in **Fig. 5 (c), (d), (e)**, few charges distributed among the interfacial Si and Cu atoms, which reveal that the weak interactions taken placed on these two atoms at the interfaces. Compared with CT-6H-SiC(0001)/Cu(111) and ST-6H-SiC(0001)/Cu(111) interfacial charge distribution, it is noted that the charges are inclined to accumulated on CT (6H-SiC(0001)/Cu(111) interfacial atoms than those of the ST (6H-SiC(0001)/Cu(111), which show that the interactions between the Cu and C atoms are stronger than those between Cu and Si atoms.

Preprints (www.preprints.org) | NOT PEER-REVIEWED | Posted: 22 December 2021 doi:10.20944/preprints202112.0359.v1

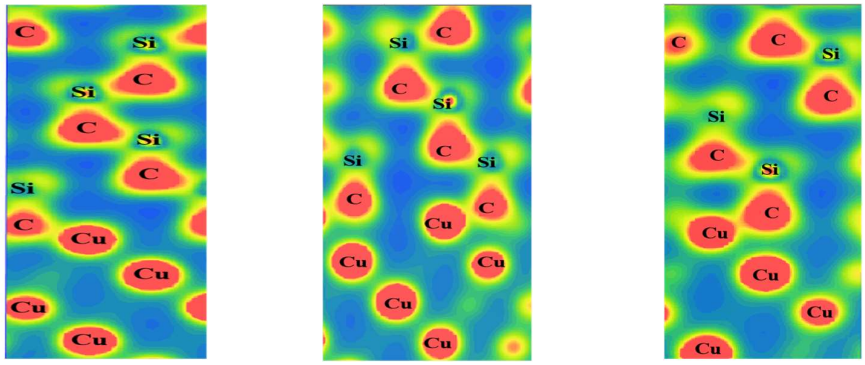

(a) CT-HCP(a) (b) CT-MT(a) (c) CT-OT(a)

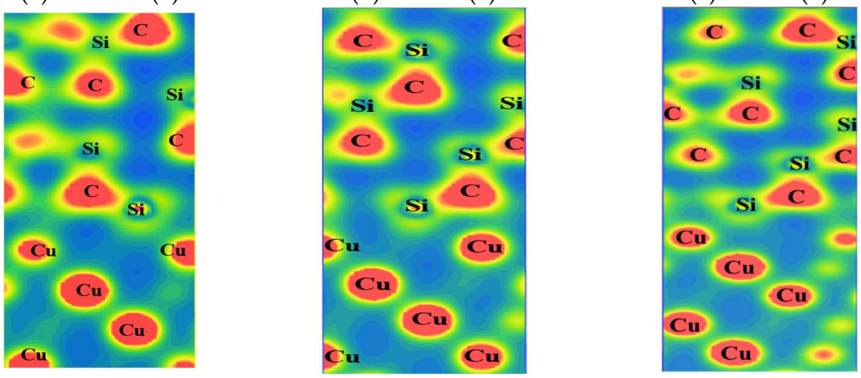

(d) ST-HCP(a) (e) ST-MT(a) (f) ST-OT(a)

Figure 5. The charge density distribution of the interfacial atoms of all "(a)" type of 6H-SiC(0001)/Cu(111) interfacial models along (211) interface (eV/Å^3).

4.2. Charge density difference of interfacial atoms of the 6H-SiC(0001)/Cu(111) interfacial atoms.

The charge density difference is applied to evaluate the charge communications between two atoms, which can be defined in following **Eq. (12)**:

$$\Delta\rho=\rho_{\text{total}}-\rho_{Cu(111)}-\rho_{SiC(0001)} \quad (12)$$

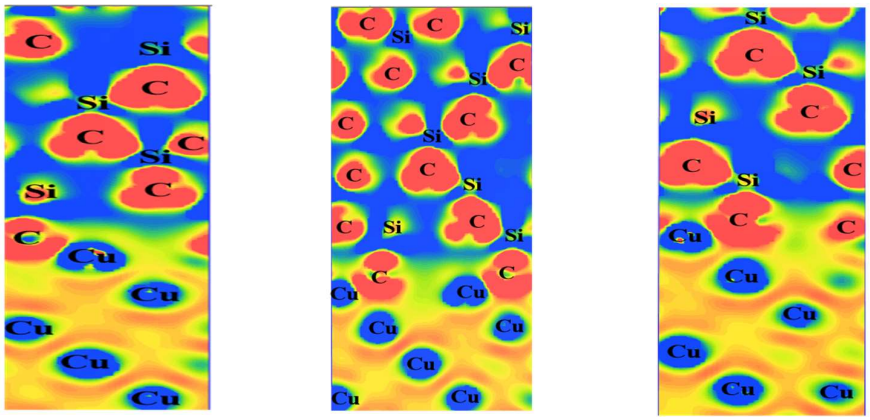

(a) CT-HCP(a) (b) CT-MT(a) (c) CT-OT(a)

Preprints (www.preprints.org) | NOT PEER-REVIEWED | Posted: 22 December 2021 doi:10.20944/preprints202112.0359.v1

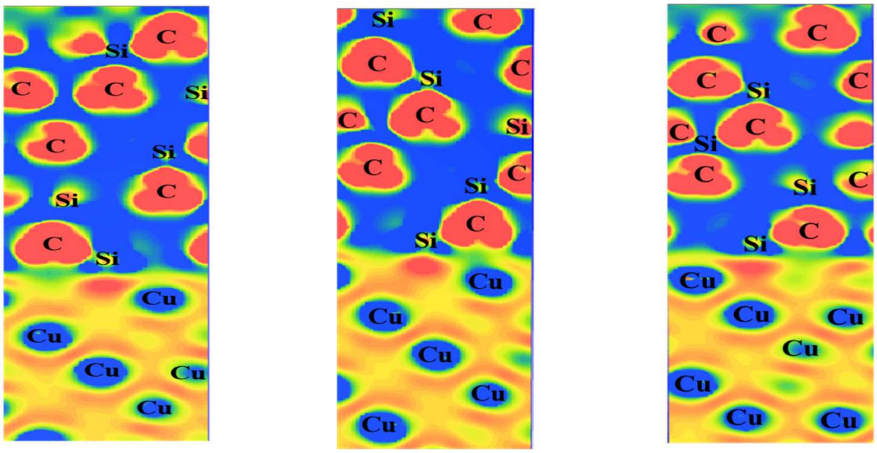

(d) ST-HCP(a) (e) ST-MT(a) (f) ST-OT(a)

Figure 6. The charge density difference of the interfacial atoms of all "(a)" type of 6H-SiC(0001)/Cu(111) interfacial models along (211) interface (eV/Å^3).

Where the ρ_{total} is the total charge density of the 6H-SiC(0001)/Cu(111) interface, $\rho_{Cu(111)}$ and $\rho_{SiC\ (0001)}$ refer to the charge densities of isolated Cu(111) and SiC(0001) slab, respectively. In **Fig. 6**, the blue color regions around Si and C atoms of the 6H-SiC indicate that few charge communications are performed in these regions. Conversely, the inter-twined yellow and red colors surrounding the Cu atoms reveal that the strong electron communications have taken places among the interior Cu atoms. The interfacial atom Cu, Si and C have obviously interacted by their charge communications, the color difference between the interfacial Cu and C atoms are more apparent than those of the interfacial Cu and Si atoms, implying that charge communication work between Cu and C atoms are stronger than those between Cu and Si atoms.

4.3. Electron localization function (ELF) of 6H-SiC(0001)/Cu(111) interfacial atoms.

The ELF is a dimensionless and its values are between the ragion 0 and 1, which evaluated the electrons localized or un-localized state between the two atoms. When the ELF equal to 1, which

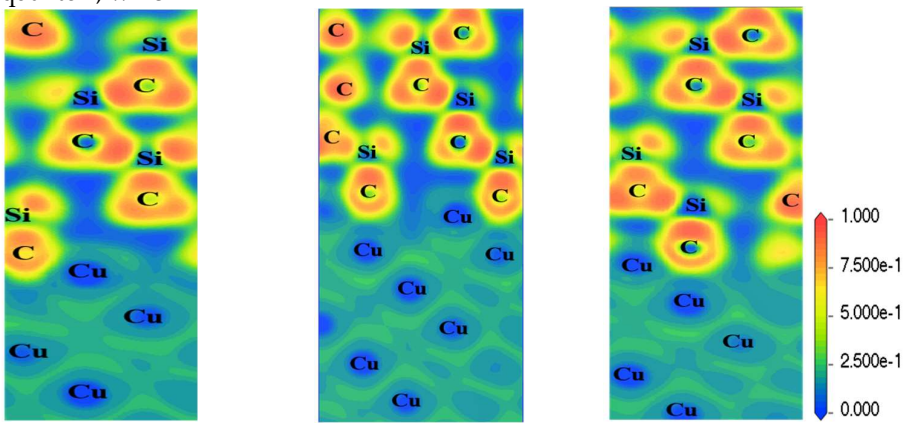

(a) CT-HCP(a) (b) CT-MT(a) (c) CT-OT(a)

Preprints (www.preprints.org) | NOT PEER-REVIEWED | Posted: 22 December 2021 doi:10.20944/preprints202112.0359.v1

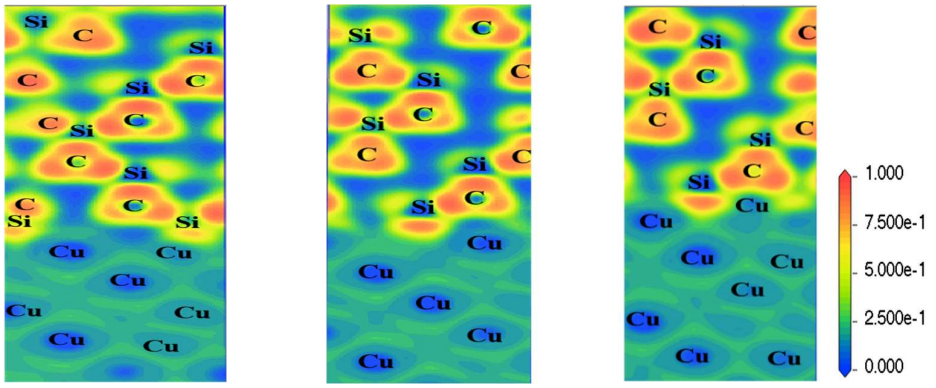

(d) ST-HCP(a) (e) ST-MT(a) (f) ST-OT(a)

Figure 7. The electron localization function of the interfacial atoms of all "(a)" type of 6H-SiC(0001)/Cu(111) interfacial models along (211) interface (eV/Å^3).

means that the electrons between two atoms are fully localized, if ELF= 0, which show that the electrons totally un-localized, if ELF is equal to the median value (0.5), which indicates that the atoms surrounded via the homogeneous electron gases [60]. In **Fig. 7**, the dark green color among the Cu atoms of the six models reveal that abundant free electrons exist in Cu interior. Nevertheless, for interior SiC of the six models, the red color between Si and C atoms showing that strong covalent bonds formed of the two atoms. In addition, the color between the interfacial Cu, C and Si atoms are quite different with those of their interior, showing that bonding state of the interfacial atoms are various with those of the interior atoms.

4.4. The partial density of state (PDOS) of 6H-SiC(0001)/Cu(111) interfacial atoms.

The partial density of state (PDOS) is applied to figure out the feature of the bonding states and electronic structures of the interfacial atoms. In this part, six 6H-SiC(0001)/Cu(111) type interfacial models are utilized to analyze the interfacial atom bonding states and their PDOS results displayed in **Fig. 8**. However, the PDOS of the other models can be seen in **Fig. SI (7) to Fig. SI (8)**. In **Fig. 8**. **(a)**, **(b)** and **(c)**, the PODS of the fist C layer atom are different with those of their interior C layer atoms, for instance, a sharp peak appeared at -10.9 eV for *s*-orbital electrons of the 1st C atoms in CT-HCP(a) and CT-MT(a) imply that the electrons belong to *s*-orbit of the 1st C atom are larger than those of the interior C atoms. Moreover, similar intensity electron of the *s*-orbit for CT-OT(a) appeared a sharp peak at -10.1 eV contrast to CT-HCP(a) and CT-MT(a).

Nevertheless, the *p*-orbital charges of the 1st C atom pass through the Fermi energy level, which show that the electrons un-localized between the interfacial C and Cu atoms. In comparison with the PDOS of interfacial and interior Cu atoms, the two peaks appeared at -1.51 eV and -1.99 eV for interior Cu atoms but which displayed at -3.74 eV and -4.69 eV for the 1st Cu atom for CT-HCP(a) (**Fig. 8(a)**). The transformed differences of these two peaks are -2.7 eV and -2.23 eV, which show that the energies decreased more obvious than those of the interior Cu atoms. In addition, owing to the hybrid of the *d*-orbital electrons of the 1st Cu atom with the *p*-orbital electrons of the

Preprints (www.preprints.org) | NOT PEER-REVIEWED | Posted: 22 December 2021 doi:10.20944/preprints202112.0359.v1

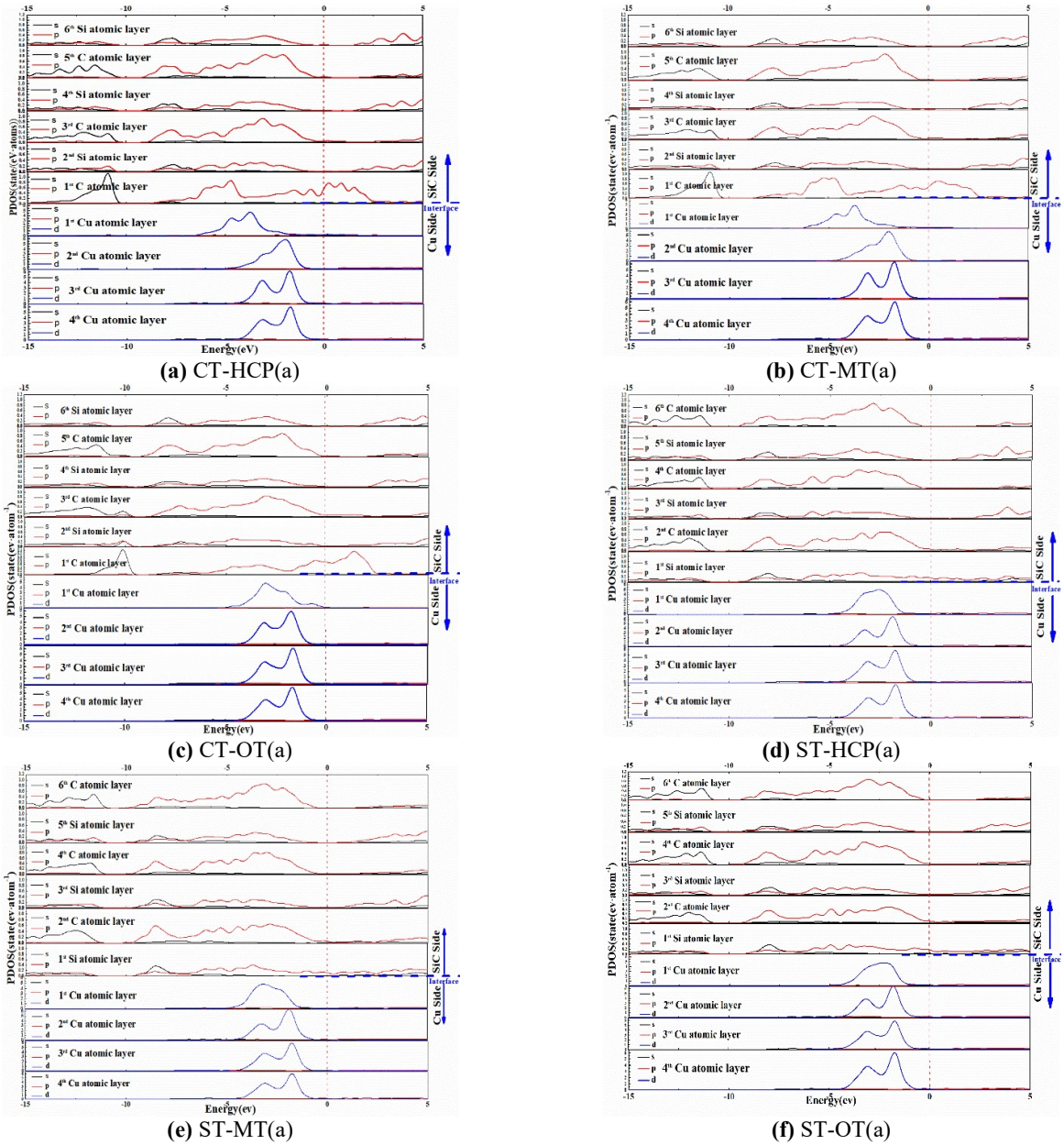

Fig.8. The partial density of state of the interfacial atoms of all "(a)" type of 6H-SiC(0001)/Cu(111) interfacial models.

1st C atoms, which lead to a C-Cu covalent bond formation. The intensities of the two peaks decreased nearly 0.91 eV/atom and 1.45 eV/atom for1st Cu atom contrasting with those of the interior Cu atoms. Nevertheless, the similar result can be obtained for CT-MT(a) and CT-OT(a), respectively.

The curves of the PDOS of the ST-6H-SiC(0001)/Cu(111) are different with those of the CT-6H-SiC(0001)/Cu(111). Taking ST-HCP(a) for instance (**Fig. 8. (a)**), although the *p*-orbital electrons pass through the Fermi energy level, only feeble intension of the *p*-orbital electrons around the Fermi energy level. Contrasting to the *s*-orbital and *p*-orbital electrons of the interior Si atoms, subtle changes happened to those of the interfacial Si atoms, which imply that the *p*-orbital electrons of the interfacial Si atoms are less influenced by *d*-orbital electrons of the interfacial Cu atoms. Moreover, the line shape of the 1st Cu *d*-orbit is neither same as the those of the CT-HCP(a), nor as those of its interior Cu atoms. In comparison with the interior Cu *d*-orbit, the line shape of the interfacial Cu *d*-orbit has wider broad peak, which formed by two peak moved to each other. Therefore, the

Preprints (www.preprints.org) | NOT PEER-REVIEWED | Posted: 22 December 2021 doi:10.20944/preprints202112.0359.v1

interactions between interfacial Si and Cu atoms are quite different with those of the C and Cu atoms, that is to say, the type bond between Si and Cu atoms are different with the bond which formed between Cu and C atoms. Moreover, the type bond formed between interfacial Si and Cu in ST-HCP(a) are formed similarly in ST-MT(a) and ST-OT(a). The PDOS of other CT-6H-SiC(0001)/Cu(111) and ST-6H-SiC(0001)/Cu(111) interfacial models have similar results obtained by CT-HCP(a) and ST-HCP(a), and they can be seen in **Fig. SI(7)** to **SI (8)**.

5. Interfacial mechanical properties

5.1. The interfacial elastic properties of 6H-SiC(0001)/Cu(111) interfaces

The elastic energy of the homogenous substance is a constant, while for heterogeneous materials are quite different [61-63]. For 6H-SiC(0001)/Cu(111) heterogeneous interfaces, the fracture toughness may tend to occur at the interface. Therefore, the interfacial fracture toughness were evaluated via the elastic energy and which defined in **Eq.(12)** [64]. In **Eq. (12),** where G_1 and G_2 refer to the shear modulus of SiC and fcc-Cu bulk, D_1 and D_2 represent the diameters of the atoms at the interface and ν_2 is the Poisson's ratio of bulk fcc-Cu. The specific interfacial elastic values of 6H-SiC(0001)/Cu(111) are displayed in **Table 5,** and it can be found that the interfacial elastic energies of the CT-6H-SiC(0001)/Cu(111) are higher than those of corresponding ST-6H- SiC(0001)/Cu(111). According to the **Table 5**, the results further testify that the interfacial stabilities of CT-6H-SiC(0001)/Cu(111) are more stable than those of the ST-6H-SiC(0001)/Cu(111).

$$\gamma_{es} = \frac{G_1 G_2 (D_1 + D_2) \mid D_1 - D_2 \mid}{2\pi D_2 (G_1 + G_2)(1+\nu_2)} \left[\ln \left[\frac{D_2}{2 \mid D_1 - D_2 \mid} \right] + 1 \right] \quad (12)$$

The assumed interfacial elastic energies are not consistent well with the sequence of the W_{ad} and γ (interfacial energies), e.g., ST-MT(c) has the largest W_{ad} (-1.32 J·m^{-2}) and lowest interfacial energy (0.273-0.600 J·m^{-2}), but its interfacial elastic energies (2.84 J·m^{-2}) neither the highest nor the lowest among the ST-6H-SiC(0001)/Cu(111) interfaces, which mainly due to the complicated circumstance of the interfaces, such as diameter of the interfacial atoms, the occupation of the interfacial atoms and the work of adhesion of the interfaces. Similar results acquired for CT-6H-SiC(0001)/Cu(111) interfaces. Therefore, it can be noted that the elastic energies of 6H-SiC(0001)/Cu(111) interfaces influenced by different atomic termination (CT or ST) are stronger

Table 5. The interfacial elastic energy of SiC(0001)/Cu(111).

Entry	atomic termination	G_1 (GPa)	G_2(GPa)	D_1(×10^{-12}m)	D_2(×10^{-12}m)	ν_2	γ_{es}(J·m^{-2})
ST-6H SiC(0001)/Cu(111)	ST-HCP(a)	191.00	78.73	263.5	361.5	0.266	2.63
	ST-MT(a)	191.00	78.73	244.5	359.6	0.266	2.88
	ST-OT(a)	191.00	78.73	197.7	357.5	0.266	3.50
	ST-HCP(b)	191.00	78.73	246.3	358.7	0.266	2.84
	ST-MT(b)	191.00	78.73	238.1	360	0.266	2.98
	ST-OT-(b)	191.00	78.73	198.4	359.2	0.266	3.52
	ST-HCP(c)	191.00	78.73	198	358.7	0.266	3.51
	ST-MT(c)	191.00	78.73	247.8	360	0.266	2.84
	ST-OT(c)	191.00	78.73	260	358	0.266	2.60
CT-6H SiC(0001)/Cu(111)	CT-HCP(a)	191.00	78.73	120.8	361	0.266	4.80
	CT-MT(a)	191.00	78.73	122.5	354.5	0.266	4.63
	CT-OT(a)	191.00	78.73	93.4	359.1	0.266	5.49
	CT-HCP(b)	191.00	78.73	123.1	353.7	0.266	4.60
	CT-MT(b)	191.00	78.73	120.5	362.1	0.266	4.83
	CT-OT(b)	191.00	78.73	121.3	360.8	0.266	4.78

Preprints (www.preprints.org) | NOT PEER-REVIEWED | Posted: 22 December 2021 doi:10.20944/preprints202112.0359.v1

	CT-HCP(c)	191.00	78.73	93.5	359.3	0.266	5.49
	CT-MT(c)	191.00	78.73	121.8	362.8	0.266	4.81
	CT-OT(c)	191.00	78.73	121.2	352.9	0.266	4.62

than those of stacking ways (HCP, MT, OT for Cu stacking and (a),(b),(c) for SiC interior structures). Specifically, the elastic energies of CT-6H-SiC(0001)/Cu(111) interfaces are about 2 J·m^{-2} larger than those of the ST-6H-SiC(0001)/Cu(111) interfaces. In addition, comparing with the same atom terminated interfaces (CT or ST-6H-SiC(0001)/Cu(111)), the difference of the elastic energies are no more than 1 J·m^{-2}, e.g., the difference of the highest (CT-OT(a)) and the smallest (CT-OT(c) elastic energy of CT-6H-SiC(0001)/Cu(111) is 0.87 J·m^{-2} (the difference of ST-6H-SiC(0001)/Cu(111) is 0.9 J·m^{-2}).

5.2. Interfacial fracture toughness of the 6H-SiC(0001)/Cu(111)

The generation of the stress transferred depending on the interfaces, ascribed to the ductile matrix to brittle reinforcement of the composites. The energy released from the crack tip zone same to the energy required to form the crack area is a necessary condition for brittle fracture under the static condition.

Table 6. The relevant interfacial fractural mechanism parameters for SiC_2/Cu interfaces (J·m^{-2}).

Entry	Interfaces	W_{ad}	γ_{es}	G_{int}	$G_{SiC(0001)}$	$G_{Cu(111)}$	$G_{int} > G_{bulk}$
ST-6H-SiC(0001)/Cu(111)	ST-HCP(a)	-1.65	2.63	-4.28	10.25	2.78(2.72 [36])	No
	ST-MT(a)	-1.39	2.88	-4.27	10.25	2.78	No
	ST-OT(a)	-1.66	3.50	-5.16	10.25	2.78	No
	ST-HCP(b)	-1.46	2.84	-4.3	10.25	2.78	No
	ST-MT(b)	-1.59	2.98	-4.57	10.25	2.78	No
	ST-OT(b)	-1.80	3.52	-5.32	10.25	2.78	No
	ST-HCP(c)	-1.55	3.51	-5.06	10.25	2.78	No
	ST-MT(c)	-1.32	2.84	-4.16	10.25	2.78	No
	ST-OT(c)	-1.37	2.60	-3.97	10.25	2.78	No
CT-6H-SiC(0001)/Cu(111)	CT-HCP-a	2.76	4.80	-2.04	10.25	2.78	No
	CT-MT-a	2.83	4.63	-1.83	10.25	2.78	No
	CT-OT-a	0.46	5.49	-5.03	10.25	2.78	No
	CT-HCP-b	2.88	4.60	-1.72	10.25	2.78	No
	CT-MT-b	3.34	4.83	-1.49	10.25	2.78	No
	CT-OT-b	2.83	4.78	-1.95	10.25	2.78	No
	CT-HCP-c	0.40	5.49	-5.09	10.25	2.78	No
	CT-MT-c	3.30	4.81	-1.51	10.25	2.78	No
	CT-OT(c)	2.88	4.62	-1.74	10.25	2.78	No

The bulk and the interface of the composites fractures can be estimated according to the Griffith theory.

$$G_{bulk} = 2\gamma_s \tag{13}$$

$$G_{int} = \gamma_{s1} + \gamma_{s2} - \gamma_{s12} - \gamma_{es} \tag{14}$$

Therefore, the work of fracture at interface for composites can be defined in **Eq. (13)** and **Eq. (14)**, in these two equations where γ_s refers to the energy of bulks, γ_{s1} represents the surface energy of the one part, γ_{s2} refers to the surface energy of the other part, γ_{s12} is the interfacial energy before the heterogeneous interfaces fractured into two faces and γ_{es} represents the interfacial elastic energy, respectively. Due to the works of adhesion are closely related the surface energies $\gamma_{Cu(111)}$, $\gamma_{SiC(0001)}$ and interfacial energies γ_{int} ($W_{ad} = \gamma_{Cu(111)} + \gamma_{SiC(0001)} - \gamma_{int}$). The **Eq. (15)** is obtained via substituting the **Eq. (10)** into the **Eq. (14)**, and which can be expressed as:

Preprints (www.preprints.org) | NOT PEER-REVIEWED | Posted: 22 December 2021 doi:10.20944/preprints202112.0359.v1

$$G_{int} = W_{ad} - \gamma_{es} \quad (15)$$

In **Eq. (14)**, the negative sign of γ_{es} represent that the two free surfaces were separated at the interface while the system sustaining the elastic energy. Before the fracture taking place, which requires $G_{bulk} > G_{int}$, when trending to break fracture, which demands that G_{bulk} is gradually approaching to G_{int}, and for absolutely breaking fractures, it gets $G_{int} > G_{bulk}$. So, when SiC/Cu interface fractured and they might apart into interior Cu matrix and SiC particles.

According to the **Eq. (13),** one can obtained the $G_{\mathrm{Cu(111)}} = 2\gamma_{\mathrm{Cu(111)}}$. Therefore, the values of the $G_{\mathrm{Cu(111)}}$ is 2.78 J·m^{-2}, which is twice of the Cu(111) slab surface energy(1.39 J·m^{-2}). However, due to the polar surface of the SiC(0001) slab, its works of fractures $G_{\mathrm{SiC(0001)}}$ are more complexes. The $G_{\mathrm{SiC(0001)}}$ can be obtained from the sum of the $\gamma_{\mathrm{SiC(0001)\text{-}Si}}$ (ST-6H-SiC(0001)/Cu(111) surface energies) and $\gamma_{\mathrm{SiC(0001)\text{-}C}}$ (CT-6H-SiC(0001)/Cu(111) surface energies), which represent the Si-terminated surface energy of the SiC(0001) and the C-terminated surfaces energy of the SiC(0001), respectively. Thus, the value of the $G_{\mathrm{SiC(0001)}}$ could be obtained via the surface energy of the SiC(0001). It can be noted that there are two region of surface energies with chemical potential of the Si atom from poor side to the rich side. So, the works of fractures $G_{\mathrm{SiC(0001)}}$ is equal to the sum of the C-terminated SiC(0001) surface energies (in **Fig. 2** which is 7.692 J·m^{-2}) and the Si-terminated SiC(0001) surface energies (in **Fig. 2** which is 2.553 J·m^{-2}) on the poor side of the Si chemical potential (the value of $G_{\mathrm{SiC(0001)}}$ is 10.245 J·m^{-2}). Similarly, the same $G_{\mathrm{SiC(0001)}}$ value 10.245 J·m^{-2} can be acquired on the rich side of the Si chemical potential, the C-terminated SiC(0001) surface energies and the Si-terminated SiC(0001) are respective as 7.367 J·m^{-2} and 2.878 J·m^{-2}. **Table 6.** displays works of fracture values of all SiC/Cu interfacial models, and their values were obtained by using of the **Eq.(14)**. According to the results in the **Table 6.**, it can be noted that all G_{int} values are negative (the values are various from -5.32 J·m^{-2} (ST-OT(b)) to -1.49 J·m^{-2} (CT-MT(b)) and which are smaller than their corresponding G_{bulk} ($G_{bulk} = \gamma_{SiC}$ =10.245 J·m^{-2} or $G_{bulk} = 2\gamma_{Cu}$ (2.78 J·m^{-2}) values. In general, based on discussion of the G_{bulk} and G_{int} mentioned above, it can be noted that the interfaces of all 6H-SiC(0001)/Cu(111) are hard to fracture.

6. Ultimate tensile strength

6.1. The ultimate tensile stress and strains of the 6H-SiC(0001)/Cu(111) interfaces

As strain increasing along the c directions of the models, the ultimate tensile stress of the various 6H-SiC(0001)/Cu(111) models could be carried out under the different ultimate strains. Therefore, to make clear of the ultimate tensile strength of the 6H-SiC(0001)/Cu(111) interfacial models, a 0.02 strain step performing on c directions until to reach the ultimate tensile stress of the 6H-SiC(0001)/Cu(111) interfaces. In order to obtain the relationships of the strain and ultimate tensile stress, the stress *vs.* strain were plotted to acquire the variation trend of the stress. In this work, the normal strain can be expressed by **Eq. (16)** [64] in terms of engineering strain.

$$\varepsilon_{\mathrm{tensile}} = (l - l_0)/l_0 \quad (16)$$

In **Eq. (16)**, Where l_0 and l refer to the primary cell length and the deformed cell length, respectively. The engineering strain yield and keep onto the interfacial supercell model in a quasi-static way. The ultimate tensile stress of the C-terminated and Si-terminated 6H-SiC(0001)/Cu(111) can be obtained via the plot of the stress vs. strain in **Fig. 9**.

Preprints (www.preprints.org) | NOT PEER-REVIEWED | Posted: 22 December 2021 doi:10.20944/preprints202112.0359.v1

The **Fig. 9 (a) (c)** contain all strains which are various from 0 to 0.32, and over the highest stress a 0.005 strains step was added to confirm the ultimate tensile stress. The **Fig. 9 (b)** and **(c)** are enlarge graphs which are marked red square in **Fig.9 (a)** and **(c)** respectively.

According to the **Fig. 9**, the plotted strain *vs.* stress of CT-6H-SiC(0001)/Cu(111) can be distinguished by their color point lines (**Fig. 9 (a)**. However, the plotted strain *vs* stress of ST-6H-SiC(0001)/Cu(111) have the same variation trend which lead to all color point lines overlapped and which cannot be distinguished (**Fig. 9 (c)**. The ultimate tensile stress for CT-6H-SiC(0001)/Cu(111) interfaces are nearly at 23 GPa (which are various from 22.11 GPa (CT-OT(b) to 23. 73 GPa (CT-HCP(c)) and their corresponding stains are different from 0.26 (CT-HCP(c)) to 0.295 (CT-HCP(b)). In addition, the ultimate tensile stress for ST-6H-SiC(0001)/Cu(111) in **Fig. 9 (d)** are about 25.5 GPa (the lowest is 25.46 GPa (ST-HCP(c) and the highest is 25.96 GPa (ST-MT(c)). The strain of

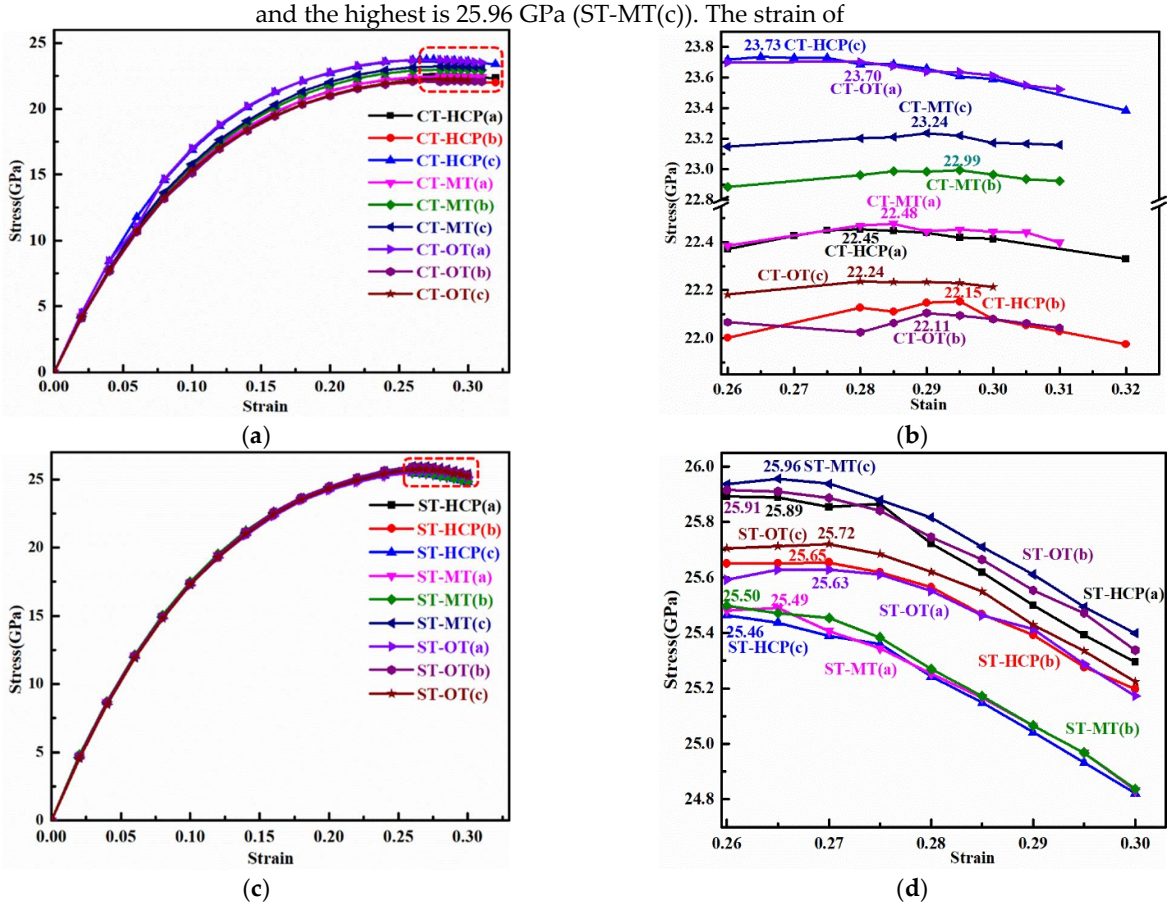

Figure 9. The strain vs. stress of the 6H-SiC(0001)/Cu(111).

corresponded to the ultimate tensile stress with the small differences for ST-6H-SiC(0001)/Cu(111) interfaces, and they are respective from 0.26 to 0.27. In comparison with the ultimate tensile stress of the ST-6H-SiC(0001)/Cu(111), the CT-6H-SiC(0001)/Cu(111) own higher ultimate tensile stress values. The strains at the ultimate tensile stress are equal to or higher than 0.28 (excepting for CT-HCP(c) (0.265)) for most of the CT-6H-SiC(0001)/Cu(111) interfaces. The strain corresponded to the ultimate tensile stress of CT-6H-SiC(0001)/Cu(111) interfaces are larger than those of the highest strain corresponded to the ultimate tensile stress 0.27 of the ST-6H-SiC(0001)/Cu(111) interfaces. The higher strain of the CT-6H-SiC(0001)/Cu(111) interfaces indicate that they have better plastic properties, which ascribe to the C-Cu formed at the interfaces. Namely, the plastic properties have been enhanced by SiC reinforcement of the copper matrix, which are mainly due to the covalent carbide are formed at the interfaces.

Preprints (www.preprints.org) | NOT PEER-REVIEWED | Posted: 22 December 2021 doi:10.20944/preprints202112.0359.v1

7. Conclusions

The SiC/Cu matrix composites were systematically investigated via the first principles. The stable properties, electronic properties and ultimate tensile strength of 6H-SiC(0001)/Cu(111) interfaces were studied and the main results are generalized as below:

(1) The work adhesion and interfacial energies of this work indicate that the CT-SiC(0001)/Cu(111) interfaces are more stable than the ST-SiC(0001)/Cu(111) interfaces.

(2) The charge density distribution, charge density difference, electron localization function and PDOS were calculated to investigate the electronic properties of 6H-SiC(0001)/Cu(111), the results indicate that covalent C-Cu bonds are formed at the CT-6H-SiC(0001)/Cu(111) interfaces, while the less interactions between the Si and Cu atoms of ST-6H-SiC(0001)/Cu(111) indicate that the valenc bonds between them are weak.

(3) The ultimate tensile strain of 6H-SiC(0001)/Cu(111) were estimated. The ultimate tensile stresses are about 23 GPa and 25 GPa for the CT-6H-SiC(0001)/Cu(111) interfaces and the ST-6H SiC(0001)/Cu(111) interfaces, respectively. Moreover, the strains corresponding to ultimate tensile strength are mostly higher than 0.28 and 0.26 for the CT-6H-SiC(0001)/Cu(111) and for ST-6H-SiC(0001)/Cu(111), respectively.

Supplementary Materials: All supplementary materials are posted online exactly as provided by the authors.

Acknowledgments: The authors appreciate the financial support from the Guangdong Academy of Science (Grant No. 2021GDASYL-20210103099), (Grant No. 2021GDASYL-20210103102), (Grant No. 2020GDASYL-20200302017), Guangdong Province Key Area R and D Program (2019B010940001), Guangzhou Science and Technology Project (202102020844), Sichuan University of Science and Engineering (2017RCL44) and the Open Project Program of Chemical Synthesis and Pollution Control Key Laboratory of Sichuan Province (Grant No. CSPC202011).

No conflicts of interest: The authors have no conflicts to disclose.

Data Availability: The data that support the findings of this study are available from the corresponding author upon reasonable request.

References

1. Wang, Y.L. ; Zhuo, L.C. ; Yin, E.-H. Progress, challenges and potentials/trends of tungsten-copper (W–Cu) composites/pseudo-alloys: Fabrication, regulation and application. Int. J. Refract. Met. H. 2021, 100, 105648.
2. Jadhav, T.; Shivanand, H. K. Investigation on mechanical and tribological properties of Boron Carbide and CNT reinforced Copper based composites. International Journal of Advance Research, Ideas and Innovations in Technology. 2019, 5, 1849-1854.
3. Franczak, A.; Baczewska, J.K. Copper matrix composites reinforced with titanium nitride particles synthesized by mechanical alloying and spark plasma sintering. Metall. Foundry. Eng 2017, 43, 97-105.
4. Chen, X.F.; Tao, J.M.; Yi, J.H.; Liu, Y.C.; Bao, R.; Li, C.J.; Tan, S.L,; You, X. Enhancing the strength of carbon nanotubes reinforced copper matrix composites by optimizing the interface structure and dispersion uniformity. Diam. Relat. Mater. 2018, 88, 74-84 (2018).
5. Sobhani, M.; Mirhabibi, A.; Arabi, H.; Brydson, R.D. Effects of in situ formation of TiB2 particles on age hardening behavior of Cu–1 wt% Ti–1 wt% TiB2. Mater. Sci. Eng. A. 2013, 577, 16-22.
6. Xiang, S.Q.; Du, X.J.; Liang, Y.H.; Zhou, M.C.; Zhang, X.F. Optimizing phase interface of titanium carbide-einforced copper matrix composites fabricated by electropulsing-assisted flash sintering, Mater. Sci. Eng. A 2021, 819, 141506.
7. Cabezas-villa, J.L.; Olmos, L.; Vergara-Hernández, H.J.; Jiménez, O.; Garnica, P.; et al. Constrained sintering and wear properties of Cu–WC composite coatings. Trans. Nonferrous Met. Soc. China. 2017, 27, 2214-2224.
8. Kang, H.K. Microstructure and electrical conductivity of high volume Al2O3-reinforced copper matrix composites produced by plasma spray. Surf. Coat. Technol. 2005, 190, 448-452.
9. Qin, Y.Q.; Tian, Y.; Zhuang, Y.; Luo, L.M.; Zan, X.; Wu, Y.C. Effects of solid–liquid doping and spark plasma sintering on the microstructure and mechanical properties of Y2O3-doped copper matrix composites. Vacuum 2021, 192, 110436.
10. Grieseler, R.; Camargo, M.K.; Hopfeld, M.; Schmidt, U.; Bund, A.; Schaaf, P. Copper-MAX-phase composite coatings obtained by electro-co-deposition: A promising material for electrical contacts. Surf. Coat. Technol. 2017, 321, 219-228.
11. Ramírez-Vinasco, D.; León-Patiño, C.A.; Nanko, M.; Aguilar-Reyes, E.A. Consolidation behaviour of Cu/AlN composites by pulse electric current sintering of copper-coated aluminum nitride precursors. Powder Technol. 2021, 377, 723–732.
12. Zhou,H.B.;Yao,P.P.; Xiao, Y.L.;et al. Friction and wear maps of copper metal matrix composites with different iron volume content. Tribology International. 2019, 132, 199-210.

Preprints (www.preprints.org) | NOT PEER-REVIEWED | Posted: 22 December 2021 doi:10.20944/preprints202112.0359.v1

13. Alaneme, K.K.; Odoni, B.U. Mechanical properties, wear and corrosion behavior of copper matrix composites reinforced with steel machining chips. Engineering Science and Technology, an International Journal. 2016, 19(3), 1593-1599.
14. Mousa, S.; Atta, M.; Abd-Elhady, A.A.; et al. Mechanical and Bond Behavior of an Advanced Quranic Metal-Matrix Composite Material (QMMC). Proceedings of the ASME 2019 14th International Manufacturing Science and Engineering Conference. Volume 2: Processes; Materials. Erie, Pennsylvania, USA. June 10–14, 2019. V002T03A084. ASME. https://doi.org/10.1115/MSEC2019-2950.
15. Dai, S.G.; Li, J.W.; Lu, N.X. Research progress of diamond/copper composites with high thermal conductivity. Diam. Relat. Mater. 2020, 108, 107993.
16. Jang, J.H.; Park, H. K.; Lee, J.H.; Lim, J.W.; Oh, I.H. Effect of volume fraction and unidirectional orientation controlled graphite on thermal properties of graphite/copper composites. Compos. B. Eng. 2020, 183, 107735.
17. Chen, L.; Hou, Z.C.; Liu, Y.F.; Luan, C.; Zhu, L.; Li, W.Z. High strength and high ductility copper matrix composite reinforced by graded distribution of carbon nanotubes. Compos. Part. A. 2020, 138, 106063.
18. Si, X.Y.; Li, M.; Chen, F.Y.; Eklund, P.; Xue, J.M.; Huang, F.; Du, S.Y.; Huang, Q. Effect of carbide interlayers on the microstructure and properties of graphene-nanoplatelet-reinforced copper matrix composites. Mater. Sci. Eng. A 2017, 708, 311-318.
19. Gupta, A.; Ghosh, T.; Jacob, C. The influence of diluent gas composition and temperature on SiC nanopowder formation by CVD. J Mater Sci. 2007,42(13):5142-5146.
20. Meng, G.; Cui, Z.; Zhang, L.; Phillipp, F. Growth and characterization of nanostructured β-SiC via carbothermal reduction of SiO2 xerogels containing carbon nanoparticles. Journal of crystal growth. 2000, 209(4), 801-806.
21. Feng, J.; Liang, S.H.; Guo, X.H.; Zhang, Y.; Song, K.X. Electrical conductivity anisotropy of copper matrix composites reinforced with SiC whiskers. Nanotechnol. Rev. 2019, 8, 285-292.
22. Asgharzadeh, H.; Eslami, S. Effect of reduced graphene oxide nanoplatelets content on the mechanical and electrical properties of copper matrix composite. J. Alloy. Compd. 2019, 806, 553-565.
23. Dhokey, N.B.; Paretkar, R.K. Study of wear mechanisms in copper-based SiCp (20% by volume) reinforced composite. Wear. 2008, 265, 117-133.
24. Brendel, A.; Woltersdorf, J.; Pippel, E.; Bolt, H. Titanium as coupling agent in SiC fibre reinforced copper matrix composites. Mater. Chem. Phys. 2005, 91, 116-123.
25. Luo, X.; Yang, Y.Q.; Liu, Y.C.; Ma, Z.J.; Yuan, M.N.; Chen, Y. The fabrication and property of SiC fiber reinforced copper matrix composites. Mater. Sci. Eng. A. 2007, 459, 244-250.
26. Akbarpour, M.R.; Salahi, E.; Hesari, F. A.; Yoon, E.Y.; Kim, H.S.; Simchi, A. Microstructural development and mechanical properties of nanostructured copper reinforced with SiC nanoparticles. Mater. Sci. Eng. A. 2013, 568, 33-39.
27. Somani, N.; Tyagi, Y.K.; Kumar, P. et al. Enhanced tribological properties of SiC reinforced copper metal matrix composites. Mater. Res. Express 2018, 6(1), 016549.
28. Rado, C.; Drevet, B.; Eustathopoulos, N. The role of compound formation in reactive wetting: the Cu/SiC system. 2000, 48, 4483-4491.
29. Dariusz, M.; Milczarek,J.M.; Wojciechowski, T. et al. The effect of metal coatings on the interfacial bonding strength of ceramics to copper in sintered Cu-SiC composites, Ceramics International. 2017, 43, 5283-5291.
30. Zhang,L.; Qu, X.H.; Duan, B.H.; et al. Microstructure and thermo-mechanical properties of pressureless infiltrated SiCp/Cu composites. Composites Science and Technology. 2008, 68. 2731-2738.
31. Chen, G.Q.; Yang, W.S.; Dong, R.H.; et al. Interfacial microstructure and its effect on thermal conductivity of SiCp/Cu composites. Mater & Design, 2014, 63,109-114.
32. Strojny-Nędza, A.; Pietrzak, K.; Teodorczyk, M.; et al. Influence of Material Coating on the Heat Transfer in A Layered Cu-SiC-Cu system. Arch. Metall. Mater. 2017, 62(2B),1311-1314.
33. Zhou, Y.G.; Hu, M. Mechanical behaviors of nanocrystalline Cu/SiC composites: An atomistic investigation. Comput. Mater. Sci. 2017, 129, 129-136.
34. Xiong, Y.; Hu, W.; Shu, Y.; Luo, X.; Zhang, Z.; He, J. ; Yin, C.; Zheng, K. Atomistic simulation on the generation of defects in Cu/SiC composites during cooling, J. Mater. Sci. Technol. (2021) accepted.
35. Zhang, K.; Zhan, Y.Z. Adhesion strength and stability of Cu(111)/TiC(111) interface in composite coatings by first principles study. Vacuum. 2019, 165, 215-222.
36. Shu, Y.; Xiong, Y.N.; Luo, X.; Zhang, Z.B.; He, J.Z.; Yin, C.C.; Ding, X.Y.; Zhang, S.W.; Zheng, K.H. Adhesion strength, stability and electronic properties of TiB2 reinforced copper matrix composites: A first principles study. Phycia B 2022, 625C, 413457.
37. Wu, Z.X.; Pang, M.J.; Zhang, Y.Z.; et al. The bonding characteristics of the Cu(111)/WC(0001) interface: An insight from first-principle calculations. Vacuum. 2021, 191, 110218.
38. Kracica,M.;Mayes,.E.L.H.;Tran,H.N.; et al. Rectifying electrical contacts to n-type 6H–SiC formed from energetically deposited carbon. Carbon. 2016, 102, 141-144.
39. Smith,S.R.; Evwaraye,A.O.;Mithel,W.C. Admittance Spectroscopy of 6H, 4H,and 15R Silicon Carbide. Phys. Stat. Sol. (A) 1997, 162, 227-238.
40. Schadt, M.; Pensl, G.; Devaty, R. P.; et al. Anisotropy of the electron Hall mobility in 4H, 6H, and 15R silicon carbide. Appl. Phys. Lett. 1994, 65, 3120-3122.

Preprints (www.preprints.org) | NOT PEER-REVIEWED | Posted: 22 December 2021 doi:10.20944/preprints202112.0359.v1

41. Segall, M.D.; Lindan, P.J.D.; Probert, M.J.; Pickard, C.J.; Hasnip, P.J.; Clark, S.J.; Payne, M.C. First-principles simulation: ideas, illustrations and the CASTEP code. J. Phys. Condens. Matter. 2002, 14, 2717-2744.
42. Clark, S.J.; Segall, M.D.; Pickard, C. J.; Hasnip, P.J.; Probert, M.J.; Refson, K.; Payne, M.C. First principles methods using CASTEP. Zeitschrift für Kristallographie. 2005, 220, 567-570.
43. Perdew, J.P.; Burke, K.; Wang, Y. et al. Generalized gradient approximation for the exchange-correlation hole of a many-electron system. Phys. Rev. B.1996, 54, 16533-16539.
44. Monkhorst, H.J.; Pack, J.D.Special points for Brillouin-zone integrations. Phys. Rev. B.1976, 13, 5188-5192.
45. Fischer, T.H.; Almlof, J.General methods for geometry and wave function optimization. J. Phys. Chem.1992, 96, 9768-9774.
46. Wu, Z.; Cohen, R.E. A More accurate generalized gradient approximation for solids. Phys. Rev. B 2006, 73, 235116.
47. Wu, Q.J.; Xie, J.P.; Wang, C.Q. ; Li, L.B.; Wang, A.Q.; Mao, A.X. First-principles study of the structure properties of Al(111)/6H-SiC(0001) interfaces. Surface Science, 2018, 670, 1-7.
48. Wu, Q.J.; Xie, J.P.; Wang, A.Q.; Wang, C.Q.; Mao, A.X. Effects of vacancies at Al(1 1 1)/6H-SiC(0001) interfaces on deformation behavior: A first-principle study. Comput. Mater. Sci. 2019, 158, 110-116.
49. Yan, Y.L.; Men, B.Q.; Liu, G.S.; Zheng, H.W. Effect of vacancies on magnetic behaviors of Cu-doped 6H-SiC. Appl. Phys. A. 2014, 117, 841-845.
50. Wang, C.Q.; Chang, D.H.; Jia, Y.; Xie, J.P. Electronic and mechanical properties of Al(100)/6H-SiC(0001) interfaces: a first-principles study. Mater. Res. Express 2019, 12, 126316.
51. Hong, M.H,; Samant, A.V.; Pirouz. P. Stacking fault energy of 6H-SiC and 4H-SiC single crystals. Philos. Mag. A. 2000, 80, 919-935.
52. Du, J.L.; Wen, B.; Melnik, R.; Kawazoe, Y. Phase stability, elastic and electronic properties of Cu–Zr binary system intermetallic compounds: a first-principles study. J. Alloy. Comp. 2014, 588, 96-102.
53. Zhu, Y.D.; Yan, M.F.; Zhang, Y.X.; Zhang, C.S. First-principles investigation of structural, mechanical and electronic properties for Cu–Ti intermetallics. Comput. Mater. Sci. 2016, 123, 70-78.
54. Ellner, M.; Kolatschek, K.; Predel, B. On the partial atomic volume and the partial molar enthalpy of aluminium in some phases with Cu and Cu3Au structures. J. Less Common Met. 1991, 170, 171-184.
55. Xu, X.Y.; Wang, H.Y.; Zha, M.; Wang, C.; Yang, Z.Z.; Jiang, Q.C. Effects of Ti, Si, Mg and Cu additions on interfacial properties and electronic structure of Al(111)/4H-SiC(0001) interface: A first-principles study," Appl. Surf. Sci. 2018, 437, 103-109.
56. Guo, W.B.; Bian, W.S.; Xue, H.T.; Zhang, X.M. Promoting wetting of Mg on the SiC surfaces by addition of Al, Zn and Zr elements: A study via first-principle calculations. J. Magnes. Alloy 2021, DOI:10.1016/j.jma.2020.12.011.
57. Zhang, W.; Smith, J.R.; Evans, A.G. The connection between ab initio calculations and interface adhesion measurements on metal/oxide systems: Ni/Al2O3 and Cu/Al2O3. Acta. Mater. 2002, 50, 3803-3816.
58. Appelbaum, J.A.; Hamann, D.R. Electronic structure of the Cu (111) surface. Solid. State Commun. 1978, 27, 881-883.
59. Zhao, G.L.; Smith, J.R.; Raynolds, J.; Srolovitz, D.J. First-principles study of the α-Al2O3(0001)/Cu(111) Interface. Interface Sci 1996, 3, 289-302.
60. Matito, E.; Silvi, B.; Duran, M.; Solà, M. Electron localization function at the correlated level. J. Chem. Phys. 2006, 125, 024301.
61. Povstenko, Y.Z. Theoretical investigation of phenomena caused by heterogeneous surface tension in solids. J. Mech. Phys. Solids. 1993, 41, 1499-1514.
62. Psakhie, S.G.; Shilko, E.V.; Grigoriev, A.S.; Astafurov, S.V.; Dimaki, A.V.; Smolin, A.Y. A mathematical model of particle-particle interaction for discrete element based modeling of deformation and fracture of heterogeneous elastic-plastic materials. Eng. Fract. Mech. 2014, 130, 96-115.
63. Wu, X.L.; Zhu, Z.T. Heterogeneous materials: a new class of materials with unprecedented mechanical properties. Mater. Res. Lett. 2017, 5, 527-532.
64. Li, Y.F.; Xiao, B.; Wang, G.L.; Sun, L.; Zheng, Q.L.; Liu, Z.W.; Gao, Y.M. Revealing the novel fracture mechanism of the interfaces of TiB2/Fe composite from a first principles investigation. Acta. Mater. 2018, 156, 228-244.